

## Three-wavelength scheme to optimize hohlraum coupling on the National Ignition Facility

P. Michel,<sup>1</sup> L. Divol,<sup>1</sup> R. P. J. Town,<sup>1</sup> M. D. Rosen,<sup>1</sup> D. A. Callahan,<sup>1</sup> N. B. Meezan,<sup>1</sup> M. B. Schneider,<sup>1</sup> G. A. Kyrala,<sup>2</sup> J. D. Moody,<sup>1</sup> E. L. Dewald,<sup>1</sup> K. Widmann,<sup>1</sup> E. Bond,<sup>1</sup> J. L. Kline,<sup>2</sup> C. A. Thomas,<sup>1</sup> S. Dixit,<sup>1</sup> E. A. Williams,<sup>1</sup> D. E. Hinkel,<sup>1</sup> R. L. Berger,<sup>1</sup> O. L. Landen,<sup>1</sup> M. J. Edwards,<sup>1</sup> B. J. MacGowan,<sup>1</sup> J. D. Lindl,<sup>1</sup> C. Haynam,<sup>1</sup> L. J. Suter,<sup>1</sup> S. H. Glenzer,<sup>1</sup> and E. Moses<sup>1</sup>

<sup>1</sup>Lawrence Livermore National Laboratory, Livermore, California 94551, USA

<sup>2</sup>Los Alamos National Laboratory, Los Alamos, New Mexico 87545, USA

(Received 14 September 2010; revised manuscript received 4 January 2011; published 25 April 2011)

By using three tunable wavelengths on different cones of laser beams on the National Ignition Facility, numerical simulations show that the energy transfer between beams can be tuned to redistribute the energy within the cones of beams most prone to backscatter instabilities. These radiative hydrodynamics and laser-plasma interaction simulations have been tested against large-scale hohlraum experiments with two tunable wavelengths and reproduce the hohlraum energetics and symmetry. Using a third wavelength provides a greater level of control of the laser energy distribution and coupling in the hohlraum, and could significantly reduce stimulated Raman scattering losses and increase the hohlraum radiation drive while maintaining a good implosion symmetry.

DOI: [10.1103/PhysRevE.83.046409](https://doi.org/10.1103/PhysRevE.83.046409)

PACS number(s): 52.57.Fg, 52.38.-r

### I. INTRODUCTION

The indirect drive approach to inertial confinement fusion relies on the efficient and well-balanced energy deposition of multiple laser beams into the wall of a cylindrical cavity (the “hohlraum”) [1]. The deposited energy is converted into soft x-rays, which implode a capsule containing thermonuclear fuel. Laser plasma instabilities (LPIs) determine the laser energy deposition into the hohlraum wall. In particular, forward- or side-scatter between laser beams crossing at the laser entrance holes (LEHs) of the hohlraum can lead to transfer of energy between cones of beams and affect the hohlraum radiation symmetry [2–6], while backscatter instabilities can cause an energy loss as well as an imbalance of the energy deposited onto the wall [7].

In the 2009 hohlraum energetics experimental campaign on the National Ignition Facility (NIF) [8–10], crossed-beam energy transfer has been used to adjust the energy balance on the hohlraum wall and achieve symmetric capsule implosions [2,3]. On the NIF, the “inner beams,” at 23.5° and 30° from the hohlraum axis and irradiating the hohlraum near its waist, are generated by a first oscillator at  $\lambda_{\text{inner}}$ ; the “outer beams,” at 44.5° and 50° from the hohlraum axis and hitting the hohlraum wall further from the capsule, have a separate oscillator at  $\lambda_{\text{outer}}$  (see Fig. 1). The beating between one inner and one outer beam creates a modulation of the refractive index in the plasma via the ponderomotive force; the modulation acts like an acoustic modulator, which can deflect the light of one beam in the direction of the other beam. The amount and direction of the deflection depends on the plasma flow in the crossing volume and on the wavelength separation between the beams. On NIF, increasing the wavelength separation  $\Delta\lambda = \lambda_{\text{inner}} - \lambda_{\text{outer}}$  leads to energy transfer from the outer to the inner beams, which increases the energy balance toward the hohlraum waist and leads to a more prolate implosion symmetry [5,11].

In this article, we propose a new scheme based on three tunable wavelengths [12] to redistribute the laser energy within the inner cones of beams, which are most prone to backscatter instabilities. In the next section, we present experimental results that show that the laser coupling to the target decreases

as more energy is transferred to the inner beams. The loss is identified as stimulated Raman scattering (SRS) on the undiagnosed 23.5° cone of laser beams; it is quantified using measurement of hot electrons, and the inferred SRS loss is consistent with the drop in coupling measured from the soft x-ray from the hohlraum. In Sec. III, we present a new radiation-hydrodynamic model coupled to a crossed-beam energy transfer model. The model matches the experimental trends and is used to design future experiments. Finally, Sec. IV details the third-color option idea, which consists in transferring energy out of the 23.5° beams (most prone to SRS) into the 30° beams (which do not show any increase in SRS even as more energy is transferred to them). We show quantitative predictions based on the hydrodynamics and crossed-beam transfer models as well as experimental trends. We estimate that the total SRS losses on NIF experiments could be reduced by  $\sim 2\text{--}3\times$  while keeping a good pole-waist implosion symmetry.

### II. INFERRING SRS ON THE 23.5° CONE

We focus on the same series of shots described in Refs. [2,3]. These experiments were done on subscale ( $\times 0.84$ ) hohlraums and with laser energies of 660 kJ. Our calculations for crossed-beam energy transfer predicted zero net transfer between the inner and outer cones of beams for a wavelength separation of 0.5 Å (the wavelength shifts  $\Delta\lambda$  quoted here are defined “on target,” i.e., after frequency tripling, in accordance with Ref. [2]). However, the SRS losses on the inner beams and their larger than expected absorption in the plasma (see Sec. III) resulted in a lack of energy deposition on the hohlraum wall by these beams, and thus in a lack of x-ray drive by the waist of the capsule. This in turn led to an oblate implosion symmetry. By increasing the wavelength shift between the cones of beams, we were able to transfer energy from the outer beams to the inner beams, and finally reached a round implosion with a wavelength shift of 1.7 Å; the implosion symmetry is measured by the Gated x-ray Diagnostic (GXD) [13,14], which measures the capsule x-ray emission at 9 keV [see Fig. 1(b)].

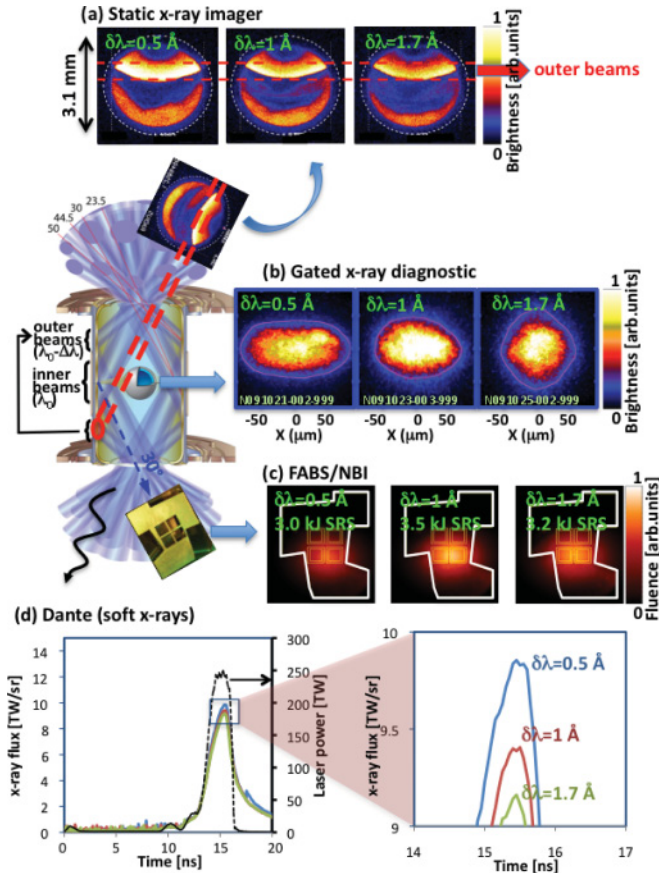


FIG. 1. (Color online) NIF hohlraum and diagnostics used to correlate LPI to hohlraum energetics (shown are the three shots at  $\Delta\lambda = 0.5, 1,$  and  $1.7 \text{ \AA}$ ): (a) the static x-ray imager (SXI) images the interior of the hohlraum wall through the LEH; (b) the gated x-ray (GXD) images show the capsule implosion symmetry; (c) the FABS/NBI system calculates backscatter on a  $30^\circ$  and a  $50^\circ$  quadruplet; and (d) Dante measures the soft x-ray emission through the LEH (also shown in black dashed line is the total laser power, same on all three shots).

The energy transfer also led to a decrease of the x-ray brightness where the outer beams hit the hohlraum wall, as measured by the static x-ray imager (SXI) [15,16] [Fig. 1(a)]. This diagnostic captures time-integrated images of the interior of the hohlraum wall x-ray emission at [3–5] keV through the LEH. As the backscatter losses on the outer beams were negligible ( $<1\%$ ), SXI provides a direct measurement of the decrease of the laser energy deposited on the hohlraum wall by the outer beams. It indicates that the outer beams energy on the wall decreased by about 30% from  $\Delta\lambda = 0.5$  to  $1.7 \text{ \AA}$ . The inner beams are not visible on the SXI; as they have half the energy of the outer beams, their relative energy increase from crossed-beam transfer can be inferred as  $\sim +60\%$ .

However, as we increased the energy transfer to the inner beams, we also measured a decrease in the soft x-ray flux, showing a decrease in laser coupling to the hohlraum as shown in Fig. 1(d). This is captured by the Dante diagnostic [17,18], which measures the x-ray spectrum from 0 to 20 keV emitted through the LEH.

On the other hand, the backscatter measurement did not indicate any significant increase in backscatter loss on the diagnosed cones of beams. Backscatter is measured by the FABS (full aperture backscatter station) and NBI (near backscatter imager) systems, installed on two quadruplets of beams on the NIF, at  $30^\circ$  and  $50^\circ$  from the hohlraum axis [19]. Negligible backscatter ( $<1\%$ ) was measured on the  $50^\circ$  quadruplet, while the  $30^\circ$  quadruplet measured a nearly constant SRS backscattered energy as  $\Delta\lambda$  was tuned from 0.5 to  $1.7 \text{ \AA}$ . The time-integrated backscatter energy was  $\sim 25 \text{ kJ}$  for the whole  $30^\circ$  cone (consisting of eight quadruplets), as shown in Fig. 1(c). No stimulated Brillouin scattering ( $<0.1\%$ ) was measured on the  $30^\circ$  beams.

A careful analysis of the hot electrons signals allowed us to identify the decrease in coupling as an increase in unmeasured SRS. The electron distribution is calculated from the measurement of the bremsstrahlung hard x-ray emitted through the hohlraum wall by energetic electrons with the Filter-Fluorescer Diagnostic System (FFLEX) [20–22]. The 10 FFLEX channels are absolutely calibrated, and their spectral responses include the detailed hohlraum composition (gold wall and aluminum case). To relate the electron energy distribution to the measured bremsstrahlung x-ray spectrum, we use the same procedure as in Ref. [23].

FFLEX measured an increase in hard x-ray signal as  $\Delta\lambda$  went from 0.5 to  $1.7 \text{ \AA}$ . The reconstructed electron distribution was best fitted using a two-temperature distribution. Fig. 2(a) shows the results of the fits for the three  $\Delta\lambda$  experiments. Each pair of points (one with  $T_{\text{hot}} \sim 10\text{--}20 \text{ keV}$  and another at  $30\text{--}60 \text{ keV}$ ) corresponds to one particular fit; any plotted fit has each of its spectral channel’s voltage within 10% of the overall best fit. In other words, the cloud of points represents all the reasonable fits to the data.

This shows that the increase in hard x-rays measured by FFLEX comes from the low-temperature part (10–20 keV) of the fit, while the high-temperature component does not show any significant change with  $\Delta\lambda$ . The low-temperature part can be attributed to SRS, while the high-temperature component probably corresponds to other instabilities occurring

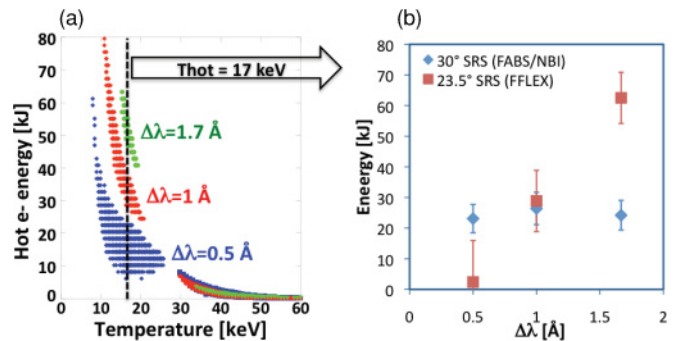


FIG. 2. (Color online) (a) Two-temperature fits from the FFLEX hot-electron diagnostic maintaining a  $<10\%$  error compared to the overall best fit. The  $30^\circ$  quadruplet SRS time-resolved spectra suggests  $T_{\text{hot}} = 17 \text{ keV}$ , from which the hot electron energy is inferred. (b) SRS energy loss in the  $23.5^\circ$  and  $30^\circ$  cones as a function of  $\Delta\lambda$ ; the  $23.5^\circ$  SRS is calculated from the hot electron energy at  $17 \text{ keV}$ , and the  $30^\circ$  SRS is measured by the FABS/NBI diagnostics.

near quarter-critical density such as two plasmon decay or forward Raman scattering. The increase in the low-temperature component can thus be explained by an increase in SRS not captured by the FABS/NBI systems. Since no SRS was measured on the outer cones (nor predicted in our simulations; see Ref. [24]), and that the  $30^\circ$  cone measured a constant backscatter loss as we tuned  $\Delta\lambda$ , we attributed the additional SRS to the undiagnosed  $23.5^\circ$  cone.

The unmeasured SRS can be estimated using the electron distribution fits from FFLEX. We assume an electron temperature for the SRS electrons equal to  $0.5mv_p^2$ , where  $m$  is the electron mass and  $v_p$  the electron plasma wave phase velocity [7,23]. Using a power-weighted average of the SRS spectrum measured by FABS to estimate  $v_p$  gives a temperature of 17 keV for the SRS-generated electron distribution (the average SRS wavelength was about 560 nm; the time-resolved spectra were very similar between the three shots). Note that this also corresponds to the maximum density of reasonable fits on Fig. 2(a). The 17 keV temperature is thus used as a constraint on the fits; for each experiment, we use all the reasonable fits at the fixed temperature of 17 keV to estimate the average electron energy from SRS and its error bar. From Fig. 2(a), we get 17 keV electron energies of  $15 \pm 7.5$  kJ,  $32.5 \pm 5$  kJ, and  $51 \pm 4$  kJ for  $\Delta\lambda = 0.5, 1,$  and  $1.7 \text{ \AA}$ , respectively. Manley-Rowe relations finally give the energy in the backscatter Raman wave at the measured SRS wavelengths. This gives a total SRS loss in the hohlraum of  $25.5 \pm 12.75$ ,  $55.25 \pm 8.5$ , and  $86.7 \pm 6.8$  for these three shots; the SRS in the  $23.5^\circ$  cone is estimated as the difference between the total SRS loss (inferred from FFLEX) and the SRS in the  $30^\circ$  cone (measured from FABS/NBI). The resulting SRS energies for the  $23.5^\circ$  and  $30^\circ$  cones are shown in Fig. 2(b).

Figure 2(b) therefore suggests that the  $23.5^\circ$  SRS backscattered energy increases from  $2.4 \pm 14.5$  kJ at  $\Delta\lambda = 0.5 \text{ \AA}$  to  $62.5 \pm 10$  kJ at  $\Delta\lambda = 1.7 \text{ \AA}$ . This corresponds to  $9 \pm 2.7\%$  total energy loss between  $\Delta\lambda = 0.5$  and  $1.7 \text{ \AA}$ , which is consistent with the  $7.1 \pm 2.5\%$  drop in peak x-ray flux observed in Dante over the same wavelength range, and confirms the  $23.5^\circ$  SRS as the source of coupling loss when we increase energy transfer from the outer beams to the inner beams.

### III. MODEL DEVELOPMENT

These experimental observations have led us to develop an integrated LPI and radiation-hydrodynamics model to design the forthcoming experiments. We use the Lasnex radiation-hydrodynamics code [25] with two improvements [26] to the standard physics model: (1) the Detailed Configuration Accounting (DCA) atomic physics model [27,28], and (2) a flux limiter  $f = 0.15$ . In NIF size hohlraums, a higher emissivity model leads to higher plasma emissivities, reducing the energy deposited in the coronal plasma and increasing soft x-ray flux measured by Dante in accordance with experimental measurements [26,29]. This model brings the SRS and SBS spectra calculated using linear gains with the LIP code [30] in good agreement with those measured by FABS. This observation validates the electron density and temperature modeling of the interior of the hohlraum.

A crossed-beam energy transfer model simultaneously calculates linear kinetic couplings between all the possible pairs among the 24 quadruplets of beams crossing at the LEH [3], i.e., 276 distinct and simultaneous ion acoustic waves associated with the beat wave of each pair of beams. The final result on energy transfer, once coupled in a time-dependent manner to the hydrodynamics codes, has been found to be within a factor of 2 compared to what is needed to match the measurements of implosion symmetry (from GXD) and x-ray brightness (from SXI). The exact error between the model and the experiments depends on the hydrodynamics model used (as different hydrodynamics models give different plasma conditions at the LEH, which in turn changes the coupling for crossed-beam transfer). In order to obtain an integrated working model that can be used to predict transfer in future experiments, we apply an “ad hoc” adjustment parameter on the coupling. This is practically done by applying a constant saturation level on the ion acoustic waves. When used with the DCA model and the flux limiter  $f = 0.15$ , we find that a saturation amplitude of  $\delta n/n = 3\text{--}4 \times 10^{-4}$  gives the best agreement with the measurements on several shots with various hohlraum sizes, laser pulse shapes, and energies. This saturation level is equivalent to a reduction of the coupling factor by a factor 2. The measured total backscatter is finally removed from the simulations input laser power after the energy transfer is applied [31].

The comparisons between the experiments and simulation results are shown in Fig. 3. The simulated SXI, GXD, and Dante show a very good agreement with the experiments. At  $0.5 \text{ \AA}$ , our model predicts negligible crossed-beam transfer ( $+1.5\%$  toward the outer cones) and an oblate implosion as observed in the experiments. The asymmetry is due to the losses on the inner beams, i.e., the high SRS and the absorption in the cold plasma ( $T_e < 2 \text{ keV}$  around the capsule), leading to a lack of x-ray drive near the waist of the capsule. The cone fraction, defined as the ratio of the inner cone energy to the total energy (after energy transfer and LPI losses), needs to be about 40–45% in order to obtain a round implosion. As  $\Delta\lambda$  is increased to  $1.7 \text{ \AA}$ , the  $\sim 60\%$  energy increase of the inner

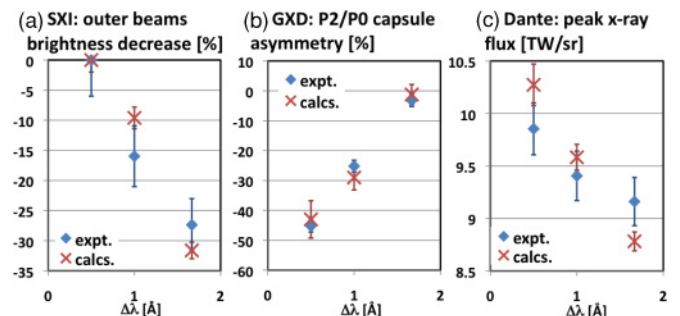


FIG. 3. (Color online) Simulated vs. measured hohlraum observables: (a) outer beams brightness from SXI (relative units); (b) P2/P0 (pole-waist) asymmetry from GXD; (c) peak x-ray flux from Dante. The error bars on the simulation results for GXD and Dante are calculated using the uncertainty on the inner beams total SRS measured with FFLEX; the SXI error bars are calculated from the brightness analysis, similarly applied to both experimental and simulated images.

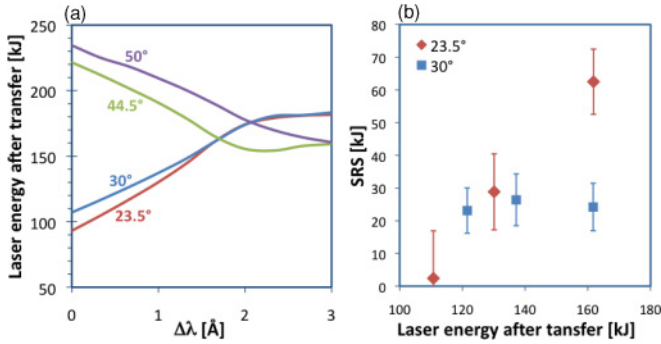


FIG. 4. (Color online) (a) Total energy in each cone of beams after crossed-beam energy transfer. (b) Total SRS loss on the 23.5° and 30° cones as a function of the energy in these cones after crossed-beam transfer.

beams from crossed-beam transfer leads to the required cone fraction for symmetric implosion; however, the increased laser energy deposition in the plasma and the increase in SRS reduce the total laser energy reaching the hohlraum wall, resulting in the drop in x-ray flux.

The model can be used to calculate the total energy in each cone of beam after energy transfer. Figure 4(a) represents the total energy in each cone of laser beams after crossed-beam energy transfer. These energies are the actual input energies for SRS; indeed, crossed-beam transfer occurs at the LEH where all the beams overlap, while SRS develops deeper inside the hohlraum at higher electron densities. Figure 4(b) shows the SRS energy as a function of laser energy after crossed-beam transfer for the 23.5° and 30° cones. This shows that the backscatter energy on the 30° cone remains constant as the laser energy increases, which means that the reflectivity actually goes down. On the other hand, the net reflectivity of the 23.5° beams goes up with increasing laser energy.

#### IV. THREE-COLOR SCHEME

These experiments have unveiled a very different behavior between the 23.5° and 30° beams SRS. This has led us to implement a third laser wavelength option on NIF. The third oscillator will seed the 23.5° cone, separately from the 30° cone and the outer cones. We will have two tunable wavelength separations:  $\Delta\lambda_{\text{out}} = \lambda_{30} - \lambda_{44.5,50}$  and  $\Delta\lambda_{23.5} = \lambda_{30} - \lambda_{23.5}$ . Note that a NBI diagnostic is also under development on a 23.5° quadruplet.

The effect of shifting  $\Delta\lambda_{23}$  while keeping  $\Delta\lambda_{\text{out}}$  fixed at 1.7 Å is shown in Fig. 5(a). A 23.5° beam has a much larger overlap volume with its two nearest 30° neighbors than with any other beam. Therefore, introducing a wavelength separation between the 23.5° and 30° beams will lead to a direct energy transfer between these two cones of beams which will be much stronger than the transfer with the outer beams for similar wavelengths separations. Thus, shifting  $\Delta\lambda_{23}$  introduces significant energy transfer from the 23.5° cone to the 30° while the outer cones stay nearly constant, as seen in Fig. 5(a). This means that we can redistribute the energy between the two inner cones with minor impact on the outer cones; we have also shown that the cone fraction

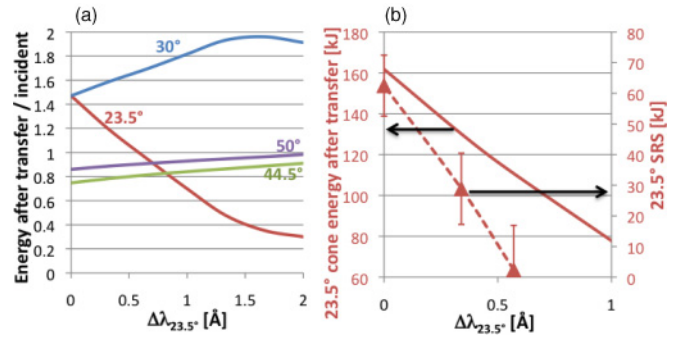


FIG. 5. (Color online) (a) Ratio of energy after to before crossed-beam transfer for each cone of beams as a function of  $\Delta\lambda_{23}$ , for a fixed  $\Delta\lambda_{\text{out}} = 1.7$  Å. (b) Solid line: energy in the 23.5° cone after crossed-beam transfer as a function of  $\Delta\lambda_{23}$ , for a fixed  $\Delta\lambda_{\text{out}} = 1.7$  Å. Triangles: resulting prediction for 23.5° SRS energy based on the experimental results of Fig. 2(b).

can be accurately readjusted by a small change in  $\Delta\lambda_{\text{out}}$  if needed.

Our strategy to improve coupling is to tune  $\Delta\lambda_{23}$  to transfer energy into the 30° beams, which do not show an increase in SRS backscattered energy versus energy transfer. The 23.5° beam SRS threshold appears to be near 110 kJ, according to Fig. 4(b). Figure 5(b) shows that a shift of  $\Delta\lambda_{23} > 0.6$  Å would bring the 23.5° below this threshold, bringing the total SRS losses back to 25 kJ and therefore recovering the 7% loss in drive when going from  $\Delta\lambda = 0.5$  to 1.7 Å [Fig. 3(c)], while preserving the overall symmetry ( $P2/P0 \sim 0$ ) since the cone fraction would not be significantly affected.

#### V. CONCLUSION

In summary, we have presented and analyzed a new scheme to control the laser beams coupling and energy deposition in greater detail in NIF experiments. A hydrodynamics and laser plasma interaction model has been developed and matches the experimental results on crossed-beam energy transfer, hohlraum drive, and capsule implosion symmetry. Detailed analysis of the 2009 National Ignition Campaign experiments suggests that the 23.5° beams SRS losses are sensitive to the laser energy after transfer, while the 30° SRS losses are not. A third wavelength option can transfer energy from the 23.5° into the 30° beams while keeping the outer beams nearly constant. Our hydrodynamics/LPI integrated model estimates that a wavelength shift of the order of 1 Å between the 23.5° and 30° beams could significantly reduce the total SRS and increase the radiation drive in the hohlraum while keeping a good pole-waist implosion symmetry. This scheme will be tested on the upcoming NIF experiments at the megajoule scale.

#### ACKNOWLEDGMENT

This work was performed under the auspices of the US Department of Energy by Lawrence Livermore National Laboratory under Contract DE-AC52-07NA27344.

- [1] J. D. Lindl, P. Amendt, R. L. Berger, S. G. Glendinning, S. H. Glenzer, S. W. Haan, R. L. Kauffman, O. L. Landen, and L. J. Suter, *Phys. Plasmas* **11**, 339 (2004).
- [2] S. H. Glenzer *et al.*, *Science* **327**, 1228 (2010).
- [3] P. Michel *et al.*, *Phys. Plasmas* **17**, 056305 (2010).
- [4] W. L. Kruer, S. C. Wilks, B. B. Afeyan, and R. K. Kirkwood, *Phys. Plasmas* **3**, 382 (1996).
- [5] P. Michel *et al.*, *Phys. Rev. Lett.* **102**, 025004 (2009).
- [6] R. K. Kirkwood, B. B. Afeyan, W. L. Kruer, B. J. MacGowan, J. D. Moody, D. S. Montgomery, D. M. Pennington, T. L. Weiland, and S. C. Wilks, *Phys. Rev. Lett.* **76**, 2065 (1996).
- [7] W. L. Kruer, *The Physics of Laser Plasma Interactions* (Westview Press, Denver, 2003).
- [8] E. I. Moses, R. N. Boyd, B. A. Remington, C. J. Keane, and R. Al-Ayat, *Phys. Plasmas* **16**, 041006 (2009).
- [9] N. B. Meezan *et al.*, *Phys. Plasmas* **17**, 056304 (2010).
- [10] S. H. Glenzer *et al.*, *Phys. Rev. Lett.* **106**, 085004 (2010).
- [11] P. Michel *et al.*, *Phys. Plasmas* **16**, 042702 (2009).
- [12] E. I. Moses and S. H. Glenzer, private communication, LLNL (2010).
- [13] J. A. Oertel *et al.*, *Rev. Sci. Instrum.* **77**, 10E308 (2006).
- [14] G. A. Kyrala *et al.*, *Rev. Sci. Instrum.* **81**, 10E316 (2010).
- [15] M. D. Landon, J. A. Koch, S. S. Alvarez, P. M. Bell, F. D. Lee, and J. D. Moody, *Rev. Sci. Instrum.* **72**, 698 (2001).
- [16] M. B. Schneider *et al.*, *Rev. Sci. Instrum.* **81**, 10E538 (2010).
- [17] H. N. Kornblum, R. L. Kauffman, and J. A. Smith, *Rev. Sci. Instrum.* **57**, 2179 (1986).
- [18] E. L. Dewald *et al.*, *Rev. Sci. Instrum.* **75**, 3759 (2004).
- [19] J. D. Moody *et al.*, *Rev. Sci. Instrum.* **81**, 10D921 (2010).
- [20] E. L. Dewald *et al.*, *Rev. Sci. Instrum.* **81**, 10D938 (2010).
- [21] J. W. McDonald, R. L. Kauffman, J. R. Celeste, M. A. Rhodes, F. D. Lee, L. J. Suter, A. P. Lee, J. M. Foster, and G. Slark, *Rev. Sci. Instrum.* **75**, 3753 (2004).
- [22] C. L. Wang, *Rev. Sci. Instrum.* **52**, 1317 (1981).
- [23] R. P. Drake, R. E. Turner, B. F. Lasinski, E. A. Williams, K. Estabrook, W. L. Kruer, E. M. Campbell, and T. W. Johnston, *Phys. Rev. A* **40**, 3219 (1989).
- [24] D. E. Hinkel, D. A. Callahan, A. B. Langdon, S. H. Langer, C. H. Still, and E. A. Williams, *Phys. Plasmas* **15**, 056314 (2008).
- [25] G. B. Zimmerman and W. L. Kruer, *Comments Plasma Phys. Control. Fusion* **2**, 51 (1975).
- [26] M. D. Rosen, Tech. Rep. LLNL-PRES\_428527 3/18/10, LLNL (2010).
- [27] Y. T. Lee, *J. Quant. Spectrosc. Radiat. Transfer* **38**, 131 (1987).
- [28] H. Scott and S. Hansen, *High Energy Density Physics* **6**, 39 (2010).
- [29] J. L. Kline *et al.*, *Phys. Rev. Lett.* **106**, 085003 (2011).
- [30] D. J. Strozzi, E. A. Williams, D. E. Hinkel, D. H. Froula, R. A. London, and D. A. Callahan, *Phys. Plasmas* **15**, 102703 (2008).
- [31] R. P. J. Town *et al.*, *Phys. Plasmas* **18**, 056302 (2011).